

Polarization-selective excitation of N-V centers in diamond

T. P. Mayer Alegre,^{1,2} C. Santori,³ G. Medeiros-Ribeiro,^{1,3} and R. G. Beausoleil³

¹*Laboratório Nacional de Luz Síncrotron, Caixa Postal 6192 - CEP 13083-970, Campinas, SP, Brazil*

²*Instituto de Física Gleb Wataghin, Universidade Estadual de Campinas, Campinas, SP, Brazil*

³*Hewlett-Packard Laboratories, 1501 Page Mill Rd., Palo Alto, California 94304, USA*

(Dated: May 28, 2018)

The nitrogen-vacancy (N-V) center in diamond is promising as an electron spin qubit due to its long-lived coherence and optical addressability. The ground state is a spin triplet with two levels ($m_s = \pm 1$) degenerate at zero magnetic field. Polarization-selective microwave excitation is an attractive method to address the spin transitions independently, since this allows operation down to zero magnetic field. Using a resonator designed to produce circularly polarized microwaves, we have investigated the polarization selection rules of the N-V center. We first apply this technique to N-V ensembles in [100] and [111]-oriented samples. Next, we demonstrate an imaging technique, based on optical polarization dependence, that allows rapid identification of the orientations of many single N-V centers. Finally, we test the microwave polarization selection rules of individual N-V centers of known orientation.

I. INTRODUCTION

Nitrogen-vacancy (N-V) centers in diamond are a promising system for implementing and testing quantum information processing protocols in solids. Spin states of single centers can be initialized and detected optically^{1,2,3,4,5}, and this capability has been extended to controlled coupling between N-V centers and other spins ($^{13}\text{C}, \text{N}$)^{6,7,8,9,10}. A special feature of this system is the spin-triplet structure of the ground states, with individual transitions that can in theory be manipulated independently using microwave polarization selection rules. The ground state of the negatively charged N-V center is known to have a (3A) spin triplet structure¹¹ which, neglecting hyperfine interactions, is described by the following electron spin Hamiltonian¹²:

$$H_e = D(S_z^2 + \frac{1}{3}S^2) + g\beta\mathbf{S} \cdot \mathbf{B}, \quad (1)$$

where \mathbf{B} is the magnetic field, $g\beta = 27.98$ GHz/T and $D = 2.88$ GHz is the zero-field splitting between the lowest-energy $m_s = 0$ sublevel, and the $m_s = \pm 1$ sublevels which are degenerate at zero magnetic field. In typical optically-detected magnetic resonance (ODMR) experiments, the microwave transitions are driven by linearly polarized fields, and individual transitions are selected by applying a magnetic field to lift the $m_s = \pm 1$ degeneracy. To avoid spin mixing, the magnetic field is usually applied along the quantization axis, which can be along any of the four $\langle 111 \rangle$ crystal axes.

An alternative method to drive the spin transitions selectively is to take advantage of polarization selection rules, since the transitions from $m_s = 0$ to $m_s = \pm 1$ occur with σ^\pm circularly polarized microwave excitation. Using polarization, rather than frequency, selective excitation at zero magnetic field becomes possible, and at weak magnetic fields where transitions still overlap (*e.g.* $B \leq 5\text{G}$) the selectivity can be improved. At small magnetic fields and under weak strain or electric field, it is expected that simultaneous cycling and non-

spin-conserving optical transitions can be realized, useful for optical readout and manipulation, respectively^{13,14}. Therefore, high selectivity and weak magnetic fields are highly desired for improving the prospects of N-V-based quantum information processing.

Here we demonstrate selective excitation of ensembles and individual N-V centers using circularly polarized microwaves for the spin transitions, and the laser polarization with respect to the N-V axis for the optical transitions.

II. EXPERIMENTAL SETUP

To test the selection rules experimentally, we performed optically-detected magnetic resonance (ODMR) experiments using a microstrip resonator designed to produce circularly polarized microwaves. The cavity is formed by two crossed microstrip resonators with orthogonal modes which generate microwaves with any polarization (from linear to circular) when the two inputs are driven with a particular phase difference (0° to 90°). Our cavity has a full-width half maximum (FWHM) resonance of 30 MHz with a quality factor of $Q = 100$. To avoid distortions from the resonance shape of the cavity, the measurements were kept within the FWHM response of the cavity. After positioning the sample above the cavity center, the resonance frequency of the cavity was trimmed by placing a low-loss dielectric above it. Three different microwave polarization configurations were used: linearly polarized, clockwise (σ^-) and counterclockwise (σ^+) circular polarizations with respect to the static magnetic field. The static magnetic field was produced by a permanent magnet placed in a linear translator close to the sample. The magnetic field direction was set along the optical detection axis (perpendicular to sample surface). Apart from the microwave polarization control, the techniques used here are similar to those used in previous room-temperature ODMR experiments^{1,11}. Fig. 1(a) shows a schematic for our ex-

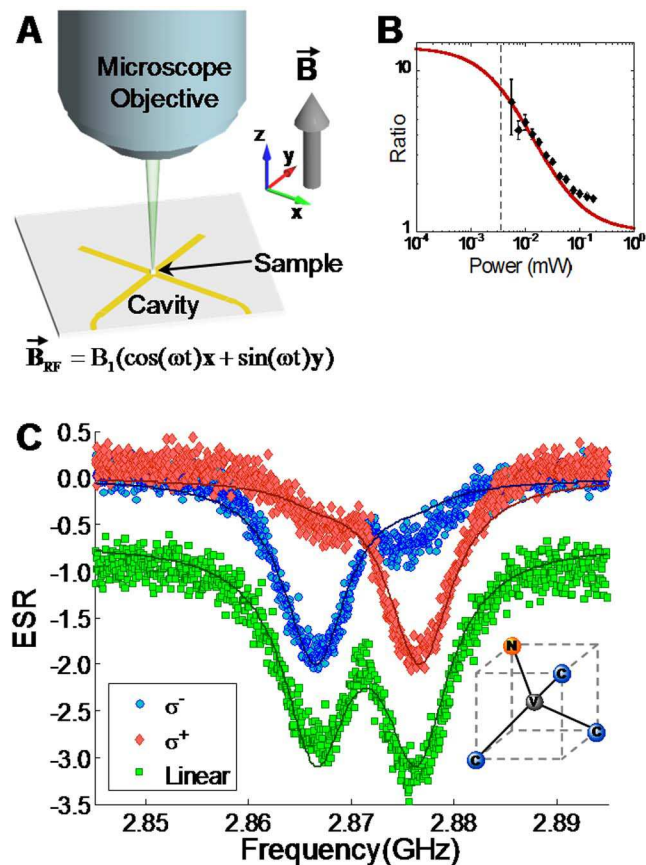


FIG. 1: **ODMR experiment on (100) sample** **a.** Schematic drawing showing the experimental positioning of the sample relative to the cavity and the magnetic field direction, which is also the rotation axis for the ac magnetic field. **b.** ODMR ratio (σ^+/σ^- amplitude) vs. microwave power intensity (points), fitted empirical equation as described in text (solid line), and saturation power (dashed line). **c.** Ensemble ODMR spectra for three microwave polarizations: σ^- (blue circles), σ^+ (red diamonds) and linear (green squares). The solid lines are fits of gaussian peaks with adjustable amplitudes and 5 MHz width. The inset is a schematic drawing showing the 4 possible N-V orientations.

perimental setup, showing the sample position above the cavity, as well as the cavity design. We used a confocal setup in which an excitation laser (532 nm) was focused to a sub-micron spot inside the sample for non-resonant excitation of the N-V centers. This setup also allowed for the control of the laser polarization incident on the sample. Laser excitation produces a spin polarization, preferentially populating the $m_s = 0$ ground state. When the applied microwave field with the appropriate polarization is resonant with one of the spin transitions, the spin polarization decreases, producing a measurable decrease in the photoluminescence intensity.

III. RESULTS AND DISCUSSION

A. [100] Oriented Sample: Ensemble Measurements

The first set of measurements (Fig. 1) was performed on a [100] oriented sample with a relatively high ($\sim 10^2 \mu\text{m}^{-2}$) concentration of N-V centers near the surface. For this crystal orientation, none of the four possible N-V orientations (Fig. 1(c), inset) have their quantization axes parallel to the surface normal, and hence a circular polarization in the laboratory frame of reference has an elliptical projection onto a plane perpendicular to the N-V axis. However the ODMR spectrum for each N-V orientation the absolute angle between the quantization axis and the surface normal is the same. The normalized transition probabilities between $m_s = 0$ to $m_s \pm 1$ are calculated theoretically to be $(2 + \sqrt{3})/12$ and $(2 - \sqrt{3})/12$, respectively.

For a quantitative verification of the selection rules we would ideally perform measurements in a regime where the microwave power dependence of the ODMR spectrum is linear. The ODMR signal dependence on the microwave power excitation can be phenomenologically described by $A = A_{max}/(1 + P_{sat}/P)$, where P_{sat} is the -3dB saturation level. Figure 1(b) shows a measurement of the resonance amplitude ratio between the two transitions ($m_s = 0 \rightarrow m_s = +1$ and $m_s = 0 \rightarrow m_s = -1$) as a function of applied microwave power. The solid line is a fit using the ratio between the two transitions, $R = (P + P_{sat}^{\sigma^+})/(P + P_{sat}^{\sigma^-})$ (for the σ^\pm microwave polarization), where in the low power limit the ratio is $P_{sat}^{\sigma^+}/P_{sat}^{\sigma^-} = (2 + \sqrt{3})/(2 - \sqrt{3})$. With these assumptions the saturation power for σ^+ is $\sim -49\text{dBm}$. Our measurements were done at -40dBm , since the time required to perform the experiment below the saturation limit at the same signal to noise ratio would be prohibitively long.

Figure 1(c) shows ESR spectra measured for three microwave polarizations, showing two peaks corresponding to the $m_s = \pm 1$ transitions. The solid lines are the calculated spectra solving Eq. 1 over the 4 possible N-V orientations, considering an inhomogeneous broadening of 7.5 MHz (obtained from the measured data) for each transition. The model does not include the saturation behavior. Circularly polarized microwave excitation produced a contrast ratio greater than 75% between the two ODMR peaks. In the linearly polarized spectrum (shifted for clarity), the slight asymmetry is due to the cavity response.

B. [111] Oriented Sample: Ensemble Measurements

Next, we describe measurements performed on a [111]-oriented sample with a much lower N-V concentration, below $1 \mu\text{m}^{-3}$. For this crystal orientation, from four possible N-V orientations (see Fig. 2(a)), one of them

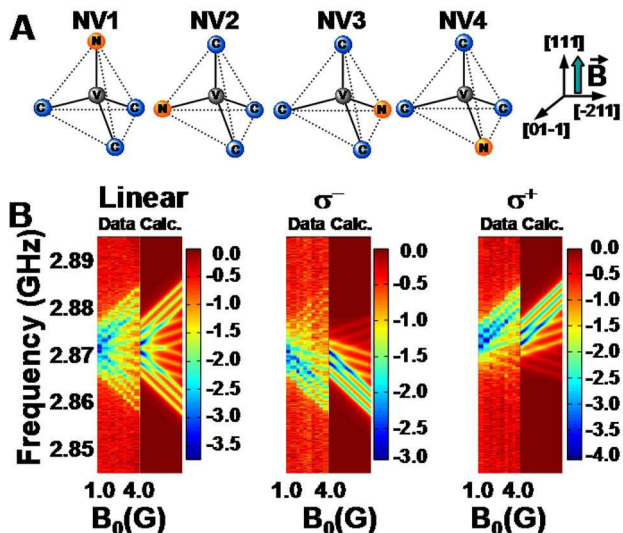


FIG. 2: Ensemble ODMR spectra for [111] oriented sample showing hyperfine interaction. a. Schematic drawing showing the relation between the 4 possible N-V orientations and the magnetic field direction. b. Color plot showing ODMR spectra vs. magnetic field (horizontal axis, from 1 to 4 gauss) and microwave frequency (vertical axis, 50MHz range) for linear, σ^- and σ^+ microwave polarizations, comparing data (left) and simulation (right) as described in the text. The simulation uses an inhomogeneous broadening of 1.2MHz to fit the data. The color scale indicates the peak depth, in percent, relative to the off-resonant case. The average number of counts, for the three measurements, is 4×10^5 .

([111], labeled “NV1”) is normal to the sample surface and is expected theoretically to exhibit perfect selection rules. For the other orientations the projected microwave field is elliptical in the N-V reference frame, and the circular selection rules are not fully observed. Thus, this measurement can reveal the orientation of a particular center. For this experimental configuration, the Zeeman splitting depends on the N-V orientation, decreasing by a factor of approximately 3 for N-V orientations other than [111].

Due to the high purity of this sample, hyperfine structure can be resolved in the ODMR spectrum. For a substitutional ^{14}N with nuclear spin $I = 1$, the Hamiltonian terms describing the nuclear Zeeman, hyperfine and quadrupole interactions are¹⁵:

$$H_T = P(I_z^2 - \frac{1}{3}I^2) - (g_n\beta_n)\mathbf{B} \cdot \mathbf{I} + \dots + A_{\parallel}S_zI_z + \frac{1}{2}A_{\perp}(S^-I^+ + S^+I^-), \quad (2)$$

where β_n is the nuclear magneton, A_{\parallel} and A_{\perp} are the hyperfine constants and P is the quadrupole splitting. Previous work^{15,16,17} has established these constants to be: $A_{\parallel} = 2.3$ MHz, $A_{\perp} = 2.1$ MHz, $g_n\beta_n = 3.07$ MHz/T and $P = -5.04$ MHz. For small static magnetic fields, the hyperfine interaction splits each of the two ODMR peaks into a triplet with splittings of approximately $A_{\parallel} =$

2.3 MHz. In this limit, each component of a triplet follows approximately the original circular polarization selection rules.

The ensemble ODMR spectra in Fig. 2(b), which show the hyperfine structure, were obtained by removing the pinhole from the collection optics to reduce spatial selectivity, and exciting with small optical and microwave powers. Measured and calculated spectra using Eq. 2 are shown. The calculation includes all possible transitions, weighted by their predicted strengths, using a lorentz function (1.2 MHz linewidth) to account for inhomogeneous broadening. For each panel in 2(b), the color scale represents the ESR intensity as a function of the static magnetic field (x-axis) and the microwave frequency (y-axis) for the three different microwave polarizations. Two different slopes are observed for the Zeeman splitting, corresponding to N-V centers oriented along [111] (steeper slope) and the other three orientations. These results exhibit good agreement between theory and experiment. For the N-V centers oriented along [111], the measured contrast ratio for σ^+ vs. σ^- excitation is approximately 9.

C. Optical determination of defect orientation

For work on single N-V centers, it is helpful to have a simple method to determine the orientation of the N-V axis. Here, we demonstrate a method based on optical polarization dependence. Since the dipole moments of the optical transitions are perpendicular to the N-V axis, the optical polarization anisotropy depends on orientation¹⁸. For a [111] sample, all four orientations can be distinguished optically, allowing rapid identification of many N-V centers through polarized scanning confocal imaging. For efficient representation of the data, we combine many images obtained with different excitation polarizations into a single image by encoding polarization into color according to the following filter function:

$$f_n(\phi) = a + \sin 2(\phi + \phi_0 + n\pi/3), \quad (3)$$

where f_n is the multiplication factor for color channel $n = 0, 1, 2$, ϕ is the polarization angle, a is an offset chosen as small as possible to maximize color saturation without producing negative pixel values, and ϕ_0 is an angle offset which controls hue. This procedure is illustrated in Fig. 3(a), where the first three panels show images obtained at the particular polarizations for which N-V orientations NV2, NV3, and NV4 have photoluminescence minima. The colors of these individual images correspond to the encoding in Eq. 3. The insets show the relative orientation of the laser polarization (\hat{L}) with respect to these three N-V axes. The minima occur when the projection of the N-V axis onto the sample surface is parallel to the electric field of the optical excitation. The last panel shows the combined image in which the four orientations can be clearly distinguished by color.

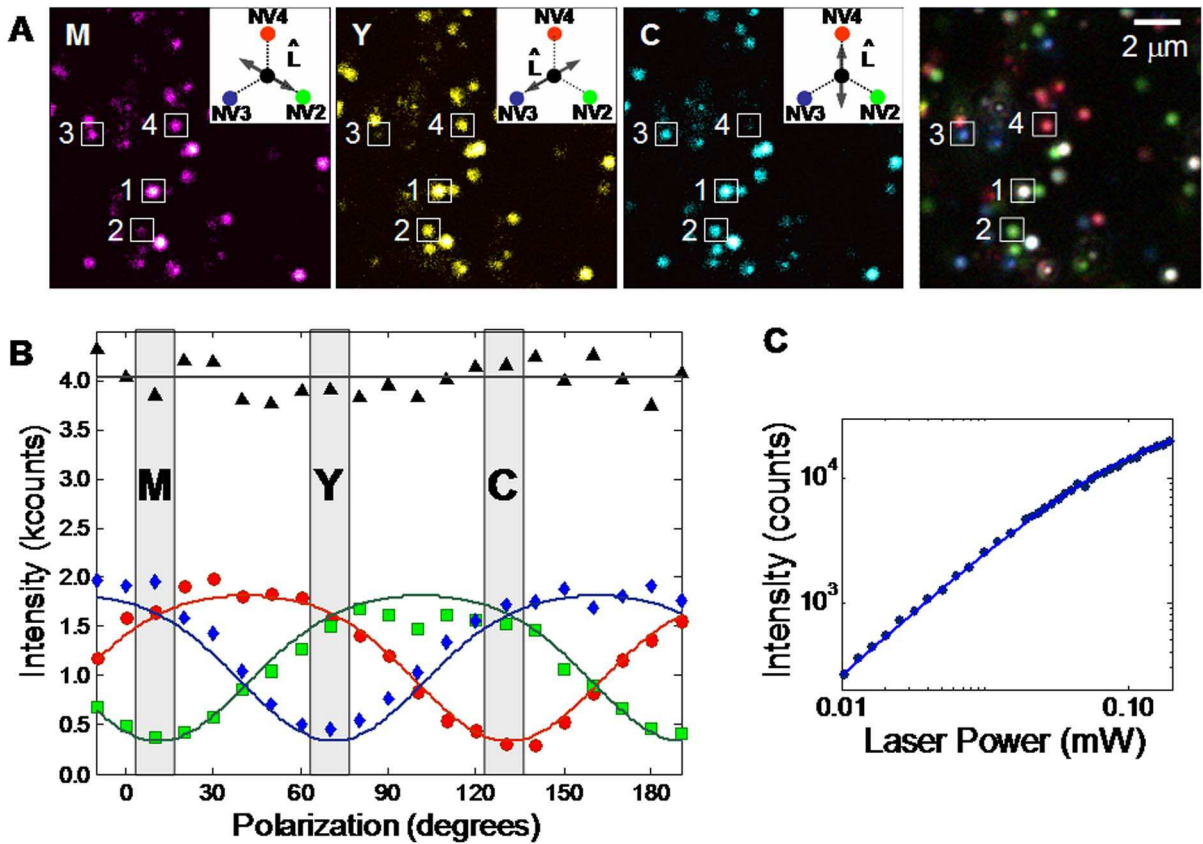


FIG. 3: **Determination of N-V orientation through optical polarization dependence.** **a.** Scanning confocal photoluminescence images showing single N-V centers, with laser polarization encoded into the three color channels MYC (magenta, yellow, and cyan). The first three images were measured for particular polarizations in which orientations designated as NV2, NV3, and NV4 have photoluminescence minima, with the electric field nearly parallel to the N-V axis. A representative N-V center of each orientation is also labeled. The fourth image is a sum over many measurement polarization angles, in which orientations NV1, NV2, NV3 and NV4 appear as white, green, blue and red, respectively. **b.** Luminescence intensity vs. excitation polarization for selected single N-V centers with orientations NV1 (black triangles, oriented normal to sample surface), NV2 (green squares), NV3 (blue diamonds), and NV4 (red circles). These measurements were performed at weak excitation power to avoid saturation of the optical transition, which distorts the polarization dependence. **c.** Excitation power dependence for a single N-V center with NV1 orientation, fitted to a simple model (solid line).

Based on photon correlation measurements, we can unambiguously associate the individual spots with single N-V centers.

The optical polarization dependence of four representative N-V centers is shown in Fig 3(b), fitted to a simple model. This model includes the effect of N-V orientation on both the excitation rate and the photoluminescence collection efficiency. For an N-V center oriented normal to the sample surface (NV1), the two dipole moments (perpendicular to the N-V axis) can be excited equally by the laser. Experimentally, for this orientation we observe that the photoluminescence is approximately unpolarized, independent of the excitation polarization (not shown). Therefore in the model we assume that the two dipole moments of the N-V center radiate with equal intensity, independent of which dipole moment is excited by the laser, a situation that would occur if relaxation between the excited states is fast at room temperature.

When both polarizations are detected as in Fig 3(b), the other orientations (NV2, NV3, NV4) produce a weaker photoluminescence signal even at maximum excitation efficiency since the collection efficiency is reduced for this geometry. The model also includes saturation of the optical transitions (measured in Fig 3(c)) and asymmetry in the collection efficiency in our setup for light polarized parallel or perpendicular to the laser polarization. Taking all of these factors into account, we obtain good agreement between theory and experiment.

D. [111] Oriented Sample: Single NV Measurements

Finally, using the method above to locate single N-V centers of known orientation, we proceed to test their microwave polarization selection rules. The ODMR spectra

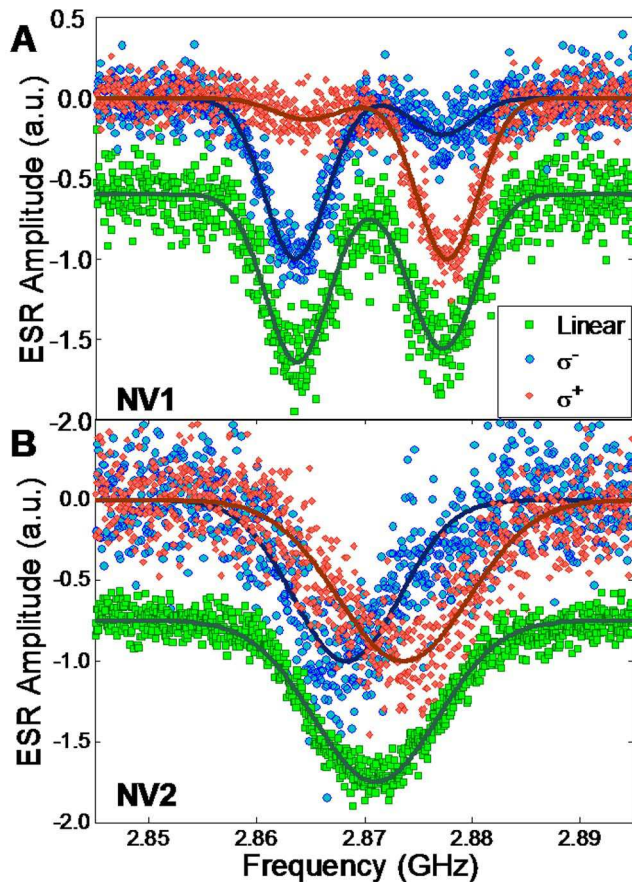


FIG. 4: **Single N-V ODMR measurements.** **a.** Signal for a single N-V center oriented along [111] (NV1) for σ^- (blue circles), σ^+ (red diamonds), and linear (green squares) microwave polarizations. The solid lines are fits using a sum of two Gaussians with adjustable amplitude. **b.** Similar measurements performed on a single center with a different orientation (NV2), fitted using a single Gaussian. The Zeeman splitting is reduced in this case because of the smaller projection ($\cos\theta = 1/3$) of the magnetic field onto the N-V axis.

for single N-V centers with NV1 and NV2 orientations are shown in Fig. 4, with data (filled symbols) and fits (solid lines). In Fig. 4(a) the fit used a superposition of two Gaussian curves corresponding to the two microwave transitions, while in Fig. 4(b) the fit used a single Gaussian since, for the smaller Zeeman splitting, the transitions are unresolved. For NV1 we expect perfect selectivity, characterized by a forbidden transition from $m = 0$ to $m = -1$ under σ^+ excitation. Experimentally, we observe a residual peak in this case with approximately 15% relative intensity which is most likely due to imperfect generation of circularly polarized microwave fields

above the cavity, or even the parasitic effect of the trimming dielectric, sample shape and microscope objective. Simulations predict that if the measurement location is just a few millimeters away from the cavity center, some ellipticity can occur. For the NV2 orientation, although the Zeeman splitting is not resolved, exciting with circular microwave polarization causes a narrowing of the transition linewidth compared with linearly polarized excitation, and a shift of the peak center is also observed, showing that the circular polarization favors one transition. Theoretically, we expect the Zeeman splitting for the NV2 orientation to be smaller by a factor of 3. We also expect reduced polarization selectivity due to the large angle between the N-V axis and the microwave polarization axis, with an additional contribution from the cross-polarized transition of 1/4 amplitude.

IV. CONCLUSIONS

In summary, we have experimentally verified spin polarization selection rules for N-V centers in diamond with various crystal and N-V orientations using circularly polarized microwave excitation. The results, including hyperfine structure, are consistent with theory. We have also demonstrated an efficient optical method for determining orientations of single N-V centers, and demonstrated microwave polarization selection rules in single N-V centers of known orientation. By optimizing the relative amplitudes and phases of the signals used to drive the two inputs of the microwave cavity, a much higher selectivity is possible. Even for the case of the [100] oriented sample, for a single N-V center, elliptically polarized excitation could in principle give perfect selectivity. Therefore we expect that microwave polarization selection rules will prove quite useful for spin manipulation, initialization and tomography of single N-V centers when improved selectively or operation at zero static magnetic field are needed.

ACKNOWLEDGMENTS

TPMA and GMR acknowledge the financial support of CNPq, FAPESP, and HP Brazil, and the technical assistance of M. H. Piazzetta and A. L. Gobbi from the micro-fabrication facility at LNLS. We also acknowledge Nobuhiko Kobayashi for XRD measurements. This work was partially supported by DARPA and the Air Force Office of Scientific Research through AFOSR contract no. FA9550-05-C-0017.

¹ A. Gruber, A. Drabenstedt, C. Tietz, L. Fleury, J. Wrachtrup, C. vonBorczyskowski, *Science* **276**, 2012-2014

(1997).

² F. Jelezko, T. Gaebel, I. Popa, A. Gruber, J. Wrachtrup

- Phys. Rev. Lett.* **92**, 076401 (2004).
- ³ F. Jelezko, I. Popa, A. Gruber, C. Tietz, J. Wrachtrup, A. Nizovtsev, S. Kilin, *Appl. Phys. Lett.* **81**, 2160-2162 (2002).
 - ⁴ F. Jelezko, and J. Wrachtrup, *J. Phys.* **16**, R1089 (2004).
 - ⁵ R. Hanson, O. Gywat, and D. D. Awschalom, *Phys. Rev. B* **74**, 161203(R) (2006).
 - ⁶ J. Wrachtrup, S. Y. Kilin, and A. P. Nizovtsev, *Optics and Spectroscopy* **91**, 429-437 (2001).
 - ⁷ F. Jelezko, T. Gaebel, I. Popa, M. Domhan, A. Gruber, J. Wrachtrup, *Phys. Rev. Lett.* **93**, 130501 (2004).
 - ⁸ T. Gaebel, *et al.*, *Nature Phys.* **2**, 408 (2006).
 - ⁹ R. Hanson, F. M. Mendoza, R. J. Epstein, D. D. Awschalom, *Phys. Rev. Lett.* **97**, 087601 (2006).
 - ¹⁰ L. Childress, M. V. Gurudev Dutt, J. M. Taylor, A. S. Zibrov, F. Jelezko, J. Wrachtrup, P. R. Hemmer, M. D. Lukin, *Science* **314**, 281-285 (2006).
 - ¹¹ E. van Oort, N. B. Manson, and M. Glasbeek, *J. Phys. C* **21**, 4385 (1988).
 - ¹² J. H. N. Loubser, J. A. Van Wyk, *Diamond Res.*, **11**, 11 (1977)
 - ¹³ N. B. Manson, J. P. Harrison, and M. J. Sellars, *Phys. Rev. B* **74**, 104303 (2006).
 - ¹⁴ Ph. Tamarat, N. B. Manson, R. L. McMurtie, N. Nitsovtsev, C. Santori, P. Neumann, T. Gaebel, F. Jelezko, P. Hemmer, J. Wrachtrup, cond-mat/0610357 (unpublished).
 - ¹⁵ F. T. Charnock, and T. A. Kennedy, *Phys. Rev. B* **64**, 041201(R) (2001).
 - ¹⁶ Xing-Fei He, N. B. Manson, and P. T. H. Fisk, *Phys. Rev. B* **47**, 8809 (1993)
 - ¹⁷ Xing-Fei He, N. B. Manson, and P. T. H. Fisk, *Phys. Rev. B* **47**, 8816 (1993)
 - ¹⁸ R. J. Epstein, F. M. Mendoza, Y. K. Kato, and D. D. Awschalom, *Nat. Phys.*, **1**, 94 (2005).